REPORT DOCUMENTATION PAGE

Form Approved
OMB No. 0704-0188

1. REPORT DATE *(DD-MM-YYYY)*	2. REPORT TYPE	3. DATES COVERED *(From - To)*
	Final Technical Report	01 Oct 2006 – 31 Aug 2007

4. TITLE AND SUBTITLE

Material Systems for Autonomous Structural Tailoring (MAST)

5a. CONTRACT NUMBER

FA9550-07-1-0002

5b. GRANT NUMBER

5c. PROGRAM ELEMENT NUMBER

6. AUTHOR(S)

Dr. Conrad Stoldt

5d. PROJECT NUMBER

5e. TASK NUMBER

5f. WORK UNIT NUMBER

7. PERFORMING ORGANIZATION NAME(S) AND ADDRESS(ES)

Department of Mechanical Engineering
University of Colorado at Boulder
Boulder CO 80309-0427

8. PERFORMING ORGANIZATION REPORT NUMBER

9. SPONSORING/MONITORING AGENCY NAME(S) AND ADDRESS(ES)

Air Force Office of Scientific Research (AFOSR)
875 N. Arlington St., Rm. 3112
Arlington, VA 22203
Dr Byung Lee/NA

10. SPONSOR/MONITOR'S ACRONYM(S)
AFOSR

11. SPONSORING/MONITORING AGENCY REPORT NUMBER
N/A

12. DISTRIBUTION AVAILABILITY STATEMENT

DISTRIBUTION A: Approved for public release; distribution unlimited.

AFRL-SR-AR-TR-07-0458

13. SUPPLEMENTARY NOTES

14. ABSTRACT

Lastly, studies were directed toward the development and modeling of collloid containing microfluidics for the active modulation of microwave absorption. A method for the self-pumping of immiscible fluids was developed and a numerical model was formulated to estimate liquid flow rates in the microchannels as a function of different parameters including device dimensions and fluid properties. Initial work also focused on the development of non-lossy injection molded microfluidic platforms fabricated from Teflon.

15. SUBJECT TERMS

16. SECURITY CLASSIFICATION OF:			17. LIMITATION OF ABSTRACT	18. NUMBER OF PAGES	19a. NAME OF RESPONSIBLE PERSON
a. REPORT	b. ABSTRACT	c. THIS PAGE			19b. TELEPONE NUMBER *(Include area code)*
Unclassified	Unclassified	Unclassified	Unclassified	15	(703)

Sponsoring Agency: DOD AFOSR
Award Number: FA9550-07-1-0002

Final Project Report

Radar Absorbing Colloidal Solutions (RACS)

Conrad R. Stoldt (PI)
Department of Mechanical Engineering, University of Colorado at Boulder

Michael H.B. Stowell (Co-PI)
Department of Molecular Biology, University of Colorado at Boulder

Zoya Popovic (Co-PI)
Department of Electrical Engineering, University of Colorado at Boulder

Albert P. Pisano and David C. Walther (Co-PIs)
Department of Mechanical Engineering, University of California at Berkeley

Project Overview

The overriding goal of the RACS project was to develop microwave active colloids whose absorptivity/reflectivity could be modulated via active and passive changes in the concentration of the nanoparticulate inclusions. Active changes were to be accomplished using immiscible fluid droplets pumped through microfluidic channels, while passive changes were to be achieved using autonomous biochemical reactions at the surface of the nanoparticles in the colloid. The microwave active colloids synthesized as part of this project were composed of iron oxide (Fe_3O_4), nickel (Ni), or copper (Cu) nanoparticles with average sizes ranging from about 10 to 100 nm, depending on the sample preparation. Molecular capping ligands were selected to impart solubility and stability in a Fluorinert FC-77 liquid matrix, and were bound to the nanoparticle surface via a carboxyl, thiol, or silane functionality on the ligand. Stable colloids were synthesized with particle volume fractions ranging from 0.01 to 10%, and it was determined that higher volume fractions were not achievable in this ligand/solvent system.

Colloidal solutions, both magnetic (Fe_3O_4 or Ni) and non-magnetic (Cu), were characterized to determine absorptive properties. Solutions of the particles, with the non-lossy Fluorinert used as the suspension liquid, were measured over a wide range of frequency bands (waveguide bands D, W, K, L & S), but no significant transmission loss was noted, or any strong reflective properties. Several methods were utilized for these measurements, including various free-space Gaussian-beam systems, and a transmission-line method. In no cases were there any statistically significant differences between the solutions with nanoparticles and those of Fluorinert alone. Based upon these initial results, it is evident that significantly higher particle volume fractions are required to achieve a microwave active cross-section, and current colloid engineering approaches remain limited to volume fractions below 10%.

Interface chemistry was implemented to modulate the aggregation and dispersion of nanoparticles in the colloid. Here, we demonstrated the controlled aggregation of Fe_3O_4 nanoparticles in organic and aqueous solutions. With decrease in solution pH, individual nanoparticles (12-14 nm) reproducibly cluster to form ~52 nm monodisperse aggregates in toluene. Spin-spin (T2) proton relaxation measurements of the micellated clusters before and after aggregation showed a change in the molar relaxation rate from 303 $sec^{-1}mol^{-1}$ to 368 $sec^{-1}mol^{-1}$ for individual and clustered nanoparticles, respectively. DNA-mediated aggregation of micellated nanoparticles in the colloidal solution was also demonstrated where the number of single-stranded DNA per particle determined the ultimate size of the nanoparticle aggregate. These results demonstrated that reversible bulk magnetic property changes in the colloid could be induced by local microscopic changes in particle density controlled by particle surface chemistry.

Lastly, studies were directed toward the development and modeling of colloid containing microfluidics for the active modulation of microwave absorption. A method for the self-pumping of immiscible fluids was developed and a numerical model was formulated to estimate liquid flow rates in the microchannels as a function of different parameters including device dimensions and fluid properties. Initial work also focused on the development of non-lossy injection molded microfluidic platforms fabricated from Teflon.

Sponsoring Agency: DOD AFOSR
Award Number: FA9550-07-1-0002

A. Introduction

Microwave absorbing materials for military applications have been investigated since the advent of radar systems. The majority of these systems, including Salisbury screens, Jaumann absorbers, radar absorbing paints, and particle laden polymeric layers, are passive in nature. There is some work with active surfaces such as variable impedance surfaces or other tunable microwave absorbers [1] and can be thought of as switched Jaumann absorbers. Furthermore, there is at least one system described in the literature [2] that modifies the change of the permittivity of an absorbing layer by introduction of a high permittivity liquid into a porous matrix of lower permittivity. The electrostatic actuation of conducting polymers can also be utilized to actively modify the absorption characteristics via application of a low strength DC bias field. The work of Wright and coworkers [3] has examined the absorptivity of polyethylene oxide polymer absorber that contains both polyanilinetetraflouroborate and silver. More recent work with poly(3,4-ethylenedioxythiophene) and copper metal in a polyethylene $LiBF_4$ polymer electrolyte matrix show that an electrical DC bias across the absorbing layer is an effective tuning mechanism for modulation of the reflected microwave signal [4]. Additional passive methods which utilize intricate miniature inductive and capacitive circuits have been demonstrated [5], however these designs have a large cost associated with their fabrication processes and limited design geometries

Recently, the feasibility of ferromagnetic nanoparticle composites for microwave absorption has been theoretically described [6, 7] and demonstrated experimentally [8, 9]. Highly efficient absorption is predicted because the composite combines the advantages of two absorbers, namely, ferromagnetic particles and a dielectric matrix. When surface area is limited (e.g., the wing of a small aircraft), the design of a good absorber becomes very difficult since precise control over some magnetic and dielectric properties is often necessitated, and conventional materials become challenging if not impossible to integrate into the design (especially at reduced scales). A composite absorber that utilizes ferromagnetic particles in combination with a dielectric matrix material offers the most flexibility for design and properties control, as the composite can be tuned and optimized via changes in both the ferromagnetic inclusions and the surrounding matrix. Ultra-small superparamagnetic (SPM) particles possess the most effective microwave absorption cross-sections [6], and through small changes in size or composition, the absorption frequency can be shifted. Similarly, the dielectric matrix can be tuned synthetically to enhance absorption. Finally, the composite as a whole can be tuned through changes in the particle volume fraction, which is demonstrated to modulate the reflected intensity of the microwave. This increase in absorption can be manifested in layers with thickness less than $\lambda/4$.

Bregar's theoretical efforts [6] indicate that the microwave reflectivity of such a nanoparticle composite can be tuned through changes in particulate volume fraction, composition, and size, or through changes in the dielectric constant of the matrix material. Experimental validation of this approach is shown by Pinho and coworkers [9], where reflection loss from a composite composed of a ~500 nm sized Co-TiBa hexaferrite filler in a polychloroprene elastomeric matrix is experimentally demonstrated in the 8-16 GHz bandwidth. Other recent work has determined the amount of RF shielding of various SPM particles (Fe_3O_4, $MnZnFe_2O_4$, and $CoFe_2O_4$) in polymer matrices at similar frequencies [8]. In conclusion, it is important to note that the simulations [6] and polymeric composites [9] report absorption effects for particle volume fractions of 10-30% and > 30%, respectively.

B. Project Results

B-1. Microwave measurement on Fe_3O_4, Ni, and Cu colloidal solutions

To measure nano-magnetic (Fe_3O_4) particles (NMPs) at a L-, S-, Ka-, W-, and D-bands, two general methods were utilized. At lower frequencies (f < 4 GHz), a transmission-line measurement experiment was configured, using a TRL (through-reflect-line) calibration to extract the complex dielectric properties of the NMPs, as well as Cu and Ni particles. Above f = 30 GHz, several free-space Gaussian-beam measurement systems were used at various bands to determine the transmission properties, from which the complex dielectric constant could be extracted. Based on all the experimental data, none of the NMPs were found to have any significant absorptive properties in any measured frequency range.

Free-space measurements

Free-space measurement systems were utilized to characterize the NMPs utilizing liquid Fluorinert (FC-77) as the mixture base. The characterized materials are listed below:

- Liquid Fluorinert (FC-77), _r = 1.9, tan(_) = 0.0036 [1];
- NMPs mixed with liquid Fluorinert with three concentrations: less than 1 mg/mL, 1 mg/mL, and 4 mg/mL;
- Colloidal Fluorinert embedded with nano-Cu particles (10% v/v);

Sponsoring Agency: DOD AFOSR
Award Number: FA9550-07-1-0002

- Liquid Fluorinert mixed with nano-magnetic (Ni) particles with concentration of 4% v/v;
- Liquid Fluorinert mixed with nano-Cu particles with 10% concentration v/v.

Since the materials for measurement are all liquid, a quartz cuvette shown in Fig. 1 was utilized to hold the liquids. The exterior dimension of the cuvette is 12.5 mm × 102.5 mm × 48 mm. Three free-space Gaussian beam measurement systems were used to characterize the listed materials: an in-house (Caltech) system operating between 30-40 GHz (shown in Fig. 2), a W-band system, and a D-band system. The latter two free-space measurement systems were used at Professor John Scales' lab at Colorado School of Mines (CSM) (shown in Fig. 3 (a) and (b)). Materials 1, 3, 4, and 5 were measured only using the in-house Gaussian beam measurement system, and materials listed in 2 were measured with all three systems.

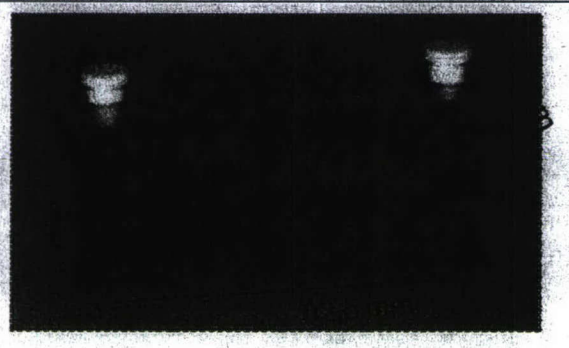

Figure 1. Quartz cuvette filled with a mixture Fluorinert and NMPs. The interior dimension is 9.5 mm × 100 mm, × 46 mm and the volume is 35.00 mL.

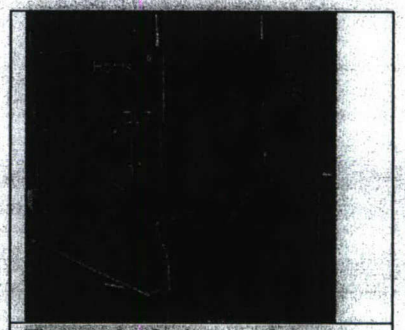

Figure 2. In-house free-space Gaussian beam measurement setup. Frequency of operation is 30-40 GHz; focal length f_0 = 30.5 cm; and lens diameter d = 33 cm.

The Caltech Measurement System

This measurement system (except for the source) was borrowed from Caltech and is set up in our lab (Fig. 2). The system has following properties:

- Frequency of operation: 30-40 GHz
- Maximum available power from the source (HP 8510C) at Ka band: 0.502 mW
- Power density at the focal plane: 0.317 W/m2
- Spot size : 12.57 cm2 (d ~ 4 cm)
- Lens diameter : 33 cm
- Focal length : 30.5 cm

Due to the lack of some optical equipment (i.e. positioners) and calibration standards, simple calibration techniques such as "response" and "response and isolation" were chosen to calibrate this system. These calibration techniques are only capable of providing either transmission response or reflection response, depending on the calibration standard. The "response and isolation" calibration technique only takes two standards: one for response, one for isolation. For the response standard, the device under test (DUT) is either removed or replaced by an empty quartz cuvette and then a thru calibration is performed. The latter is more desirable since the result contains only the transmission properties of the measured liquid. The isolation standard can be obtained by placing an absorber instead of the DUT and then performing the isolation calibration. The free-space Gaussian beam measurement system can be simulated using the transmission line model of a plane wave, since there is a plane of constant phase across the Gaussian beam spot at its focus.

The measurement first was performed on liquid Fluorinert. Since the properties of Fluorinert and the quartz cuvette are well known, a simple simulation of the system with transmission line model of a plane wave was completed. Fig. 3(a) and 3(b) show the simulated and measured transmission response of Fluorinert inside a quartz cuvette when the cuvette is not calibrated out (a) and when the cuvette is calibrated out (b). As shown in these figures, the measured transmission response follows the same trend as the simulation results but is shifted to higher than zero; this is due

Sponsoring Agency: DOD AFOSR
Award Number: FA9550-07-1-0002

to the focusing properties of the liquid and quartz. Both simulated and measured results show that Fluorinert is a low loss material at 30-40 GHz. Fig. 3(c) shows the transmission response of the empty quartz cuvette for comparison purposes.

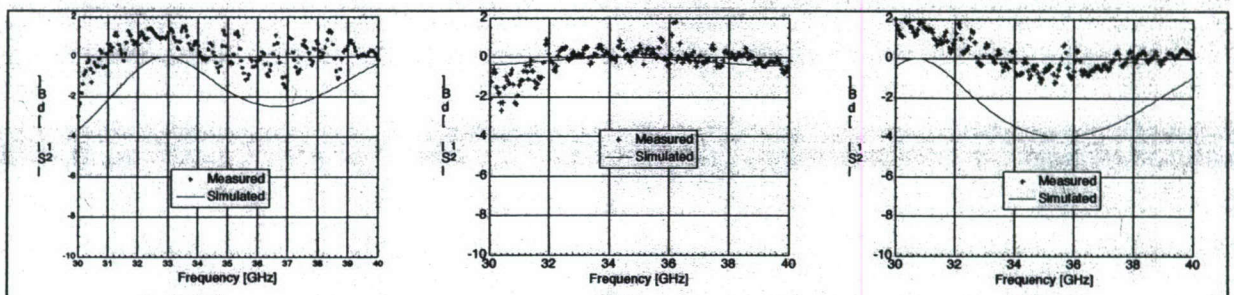

Figure 3. Simulated and measured results of the transmission response of (a) Fluorinert inside a quartz cuvette, (b) Fluorinert (quartz cuvette is calibrated out), (c) empty cuvette.

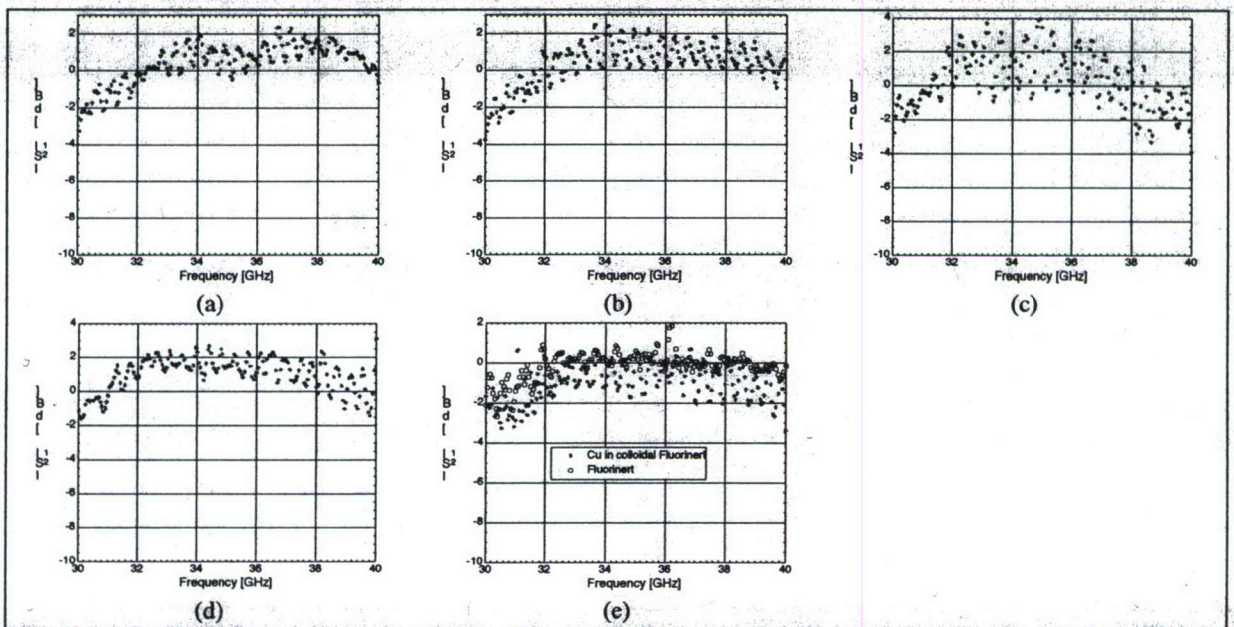

Figure 4. Measured results of the magnitude of the transmission response of (a) 4 mg/ml nano-magnetic particles (Fe_3O_4) in Fluorinert, (b) 1 mg/ml nano-magnetic particles (Fe_3O_4), (c) 4% v/v nano-Nickel particles in Fluorinert, (d) 10% v/v nano-Cu particles in Fluorinert, and (e) Cu particles in colloidal Fluorinert and unmodified Fluorinert.

The various colloidal solutions previously described were also characterized utilizing this free-space Gaussian beam measurement system. Fig. 4 shows the measured transmission response of these liquids. Since the properties of the materials were not known no simulation was performed. As shown in Fig. 4, none of these materials have significant sharp absorptive properties. Their transmission responses are very close to plain Fluorinert. Fig. 4(e) shows the comparison between Copper particles inside Fluorinert and Fluorinert itself. The reason that the transmission responses of these materials exceed above zero as mentioned before is that these materials have focusing properties.

CSM Free-space Measurement Systems

There are two Gaussian beam measurement systems (W-band and D-band) available at Professor John Scales' lab at CSM. The precise properties (i.e. focal length, spot size, lens diameters, available power from the source, etc) of these systems are not known. We know that the spot sizes of the two systems are less than 2 cm in diameter that makes the quartz cuvette large enough to use for these systems. The sample holder for the DUT is at a fixed plane,

Sponsoring Agency: DOD AFOSR
Award Number: FA9550-07-1-0002

so knowledge of the focal length is not required. The source is a millimeter-wave network analyzer (AB Millimetre). Fig. 5 shows the W-band system under test (a) and the two W- and D-band horns (b).

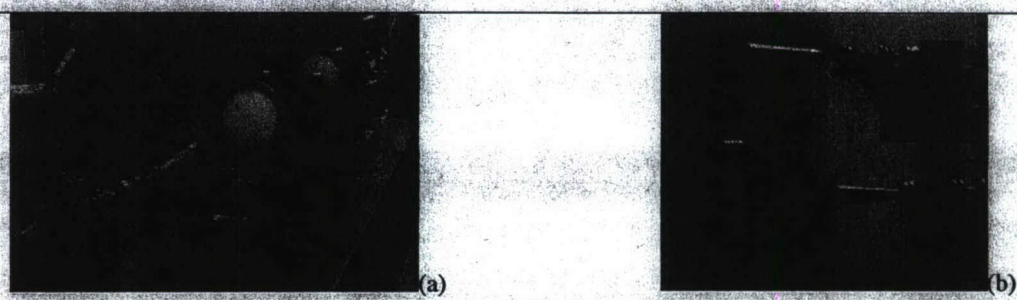

(a) (b)

Figure 5. (a) W-band Gaussian measurement system during measurement. (b) W-and-D-band horns.

The systems are capable of measuring both transmission response and reflection response. The calibration is fairly simple; an empty quartz cuvette or a reflector like an aluminum block which is larger than the spot size is placed at the focal plane, and then a through and reflect calibration is performed. In order to verify the calibration an empty quartz cuvette was measured after calibration. Fig. 6 shows the transmission and reflection response of the cuvette at W-band. The standing waves shown in the reflection response of the empty cuvette are due to the 10 mm path in the empty cuvette. As stated before the reflection calibration is done utilizing a perfect reflector (at the focal plane) so the path inside the empty cuvette is not calibrated out. The standing waves shown in the following Fig. 7 and 8 are due to the same reason.

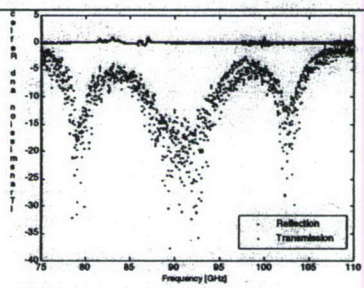

Figure 6. Magnitude of transmission and reflection responses of an empty quartz cuvette.

Iron oxide colloids were characterized using these two systems. Figures 7 and 8 show the magnitude of transmission and reflection response of these materials at D- and W-band respectively. As shown in these figures, there are no significant absorptive properties in any of the results. The solution with more concentrated materials (4mg/mL Fe_3O_4 in Fluorinert) was difficult to characterize precisely, since the particles were settling down quickly during the measurement. The magnitude of the transmission response is higher than zero because Fluorinert has focusing property; it basically performs like a lens.

TRL Calibration

TRL (through, reflect, line) is a calibration technique for circuit topologies where matched loads are difficult to obtain. This method requires three standards: a through connection, a high reflectivity termination, and a section of uniform line. The reflection coefficient of the short is not required and it can be determined during the calibration process. Also, the precise electrical length of the line standard is not required. However, the characteristic impedance, Z_0, of the delay line is a critical parameter that is necessary to be well known. TRL calibration accounts for the imperfections of the various measurement circuit components such as connectors, cables, etc. This technique is based on an 8-term error model shown in Fig. 9. TRL calibration is capable of determining the propagation and attenuation constants of the line standard. The attenuation constant is based on both conductor and dielectric losses.

Sponsoring Agency: DOD AFOSR
Award Number: FA9550-07-1-0002

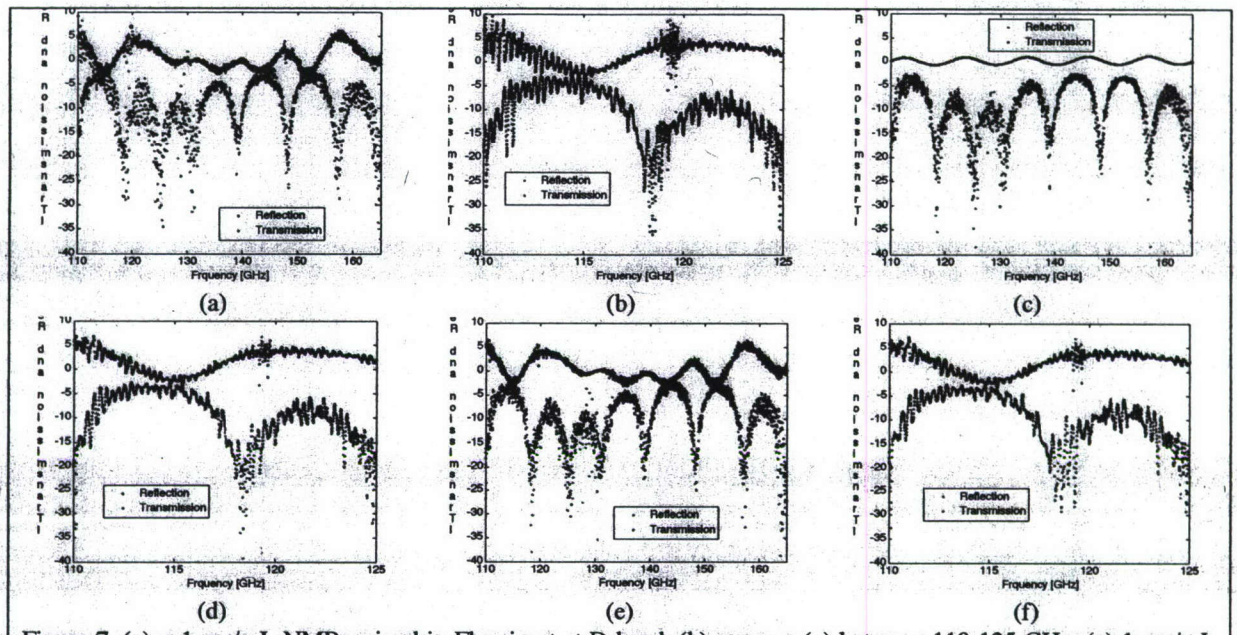

Figure 7. (a) < 1 mg/mL NMPs mixed in Fluorinert at D-band, (b) same as (a) between 110-125 GHz, (c) 1 mg/mL of NMPs in Fluorinert at D-band, and (d) same as (c) between 110-125 GHz (e) 4 mg/mL of NMPs in Fluorinert at D-band, and (f) same as (e) between 110-125 GHz .

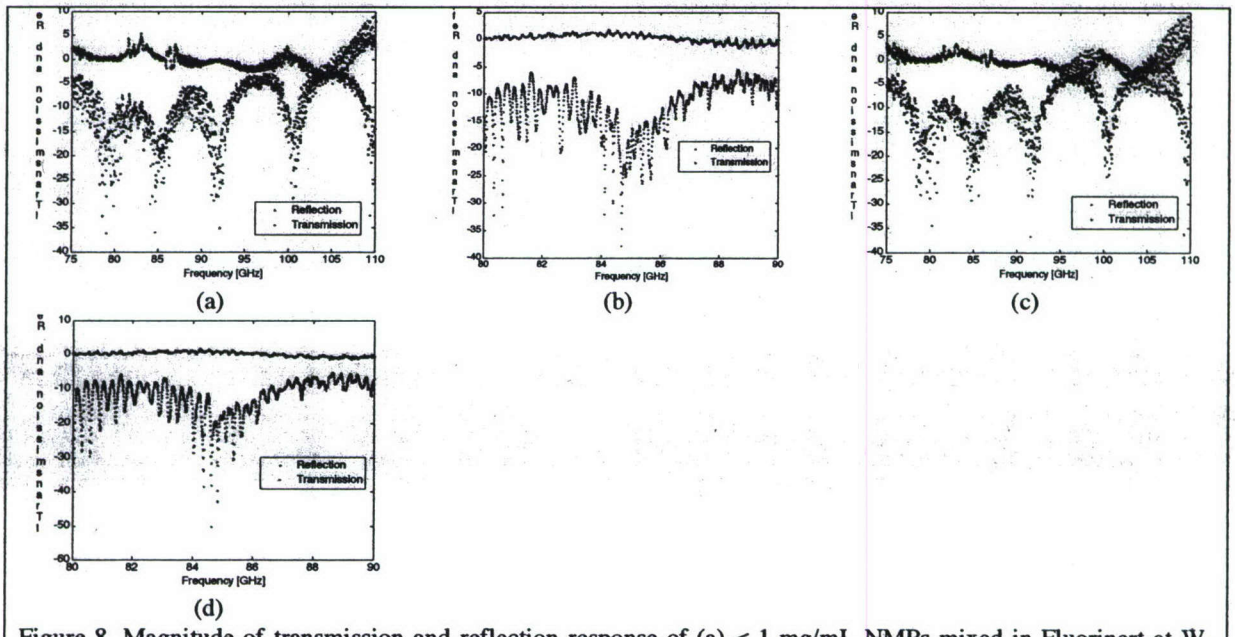

Figure 8. Magnitude of transmission and reflection response of (a) < 1 mg/mL NMPs mixed in Fluorinert at W-band, (b) same as (a) between 80-90 GHz, (c) 4 mg/mL of NMPs in Fluorinert at W-band, and (d) same as (c) between 80-90 GHz.

TRL calibration standards were designed on a multi-layered microstrip consisting of two dielectrics, either plain Fluorinert (_, = 1.9, thickness = 1 mm) or Fluorinert with NMPs, and RO 4350B (_, = 3.6, thickness = 0.338 mm). Fig. 10 shows the fabricated standards. Ansoft Designer was used to find the width of a 50 μ line on the multi-layer substrate. The width of a 50 μm line on this substrate is 4.1 mm. The physical length of the through standard is 69 mm; the short standard is 69/2 = 34.5 mm long, and the line standard is 87 mm.

Sponsoring Agency: DOD AFOSR
Award Number: FA9550-07-1-0002

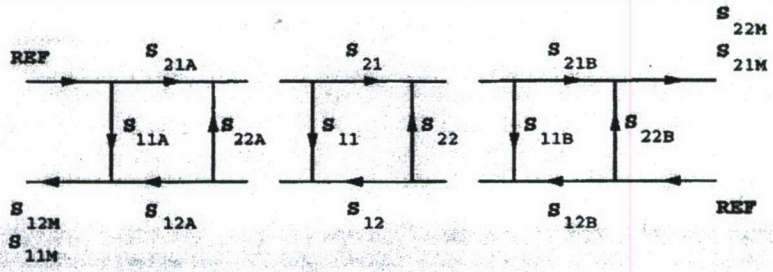

Figure 9. TRL error model. The left- and right-most graph paths with subscripts 'A' and 'B' correspond to the error matrices of any part of the circuit, from either port of measurement, up to the reference plane where the device (central graph section) is located.

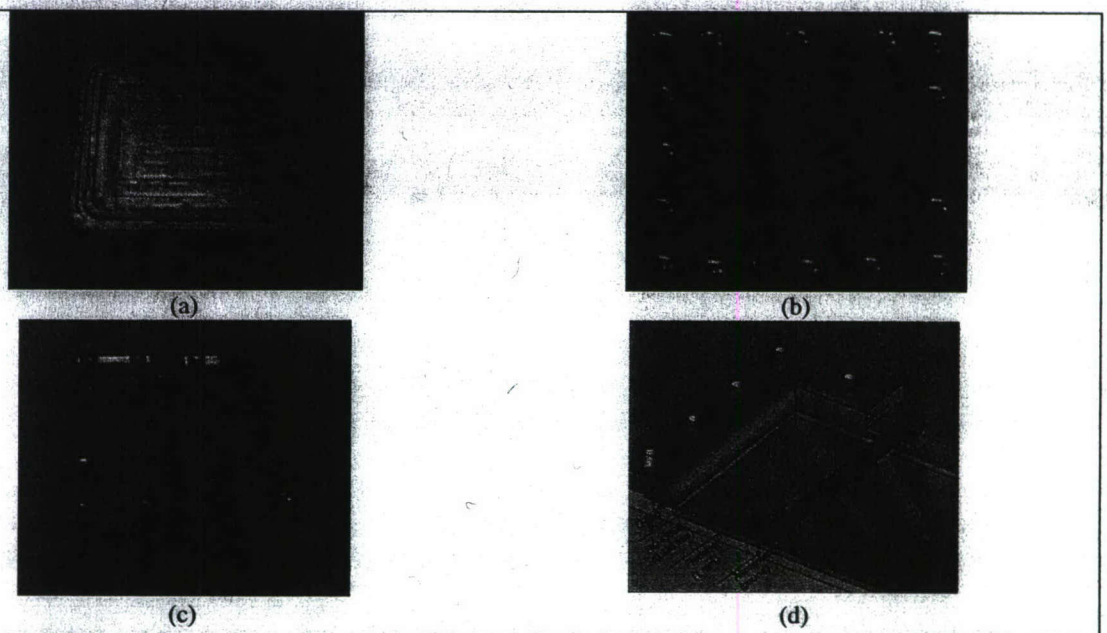

Figure 10. (a) Fabricated fixture base of thru and refelect standards, it contains a 1 mm deep pool for liquid and an o-ring groove. (b) Completed thru and reflect standard, the width of the lines is 4.1mm. (c) The line standard; 18 mm longer than thru. (d) Rendered cross-section of a standard indicating each layer.

Two sets of measurements were performed on the fabricated standards using an HP 8510C VNA and its built-in TRL function. In the first measuremt Fluorinert was used as the liquid layer in the standards. At first the TRL calibration was performed using the fabricated standards, that means the effect of the connectors and the o-ring was calibrated out. Fig. 11 shows the S-parameters of the "line" after calibration. Note that the "line" is only 18 mm long which is the difference between the line standard and thru. The complex propagation constant and the attenuation constant of the line has been extracted from the measured S_{21} of the line. Figure (4) shows these results. As shown in Fig. 12 (a) the attenuation constant (_) is less than 0.1 dB/cm which means that Fluorinert is a low loss liquid at this frequency band (1-4 GHz). The propagation constant (_) (shown in Fig. 12 (b) is increasing linearly with respect to frequency as expeceted.

The second sets of measurements were performed when Fluorinert with de-embeded NMPs (1 mg/ mL) was used to fill the liquid layer in the standards. Fig. 13 shows the S-parameters of the line. Fig 14 shows the attentuation and propagation constant of the line. These parameters are almost identical to the results when plain Fluorinert was used as the liquid. This means that the NMPs do not have absorptive properties between 1-4 GHz.

Sponsoring Agency: DOD AFOSR
Award Number: FA9550-07-1-0002

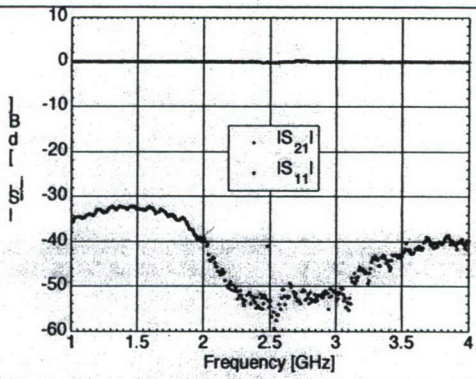

Figure 11. Magnitude of S21 and S11 of the line standard when the standard are filled with Fluorinert.

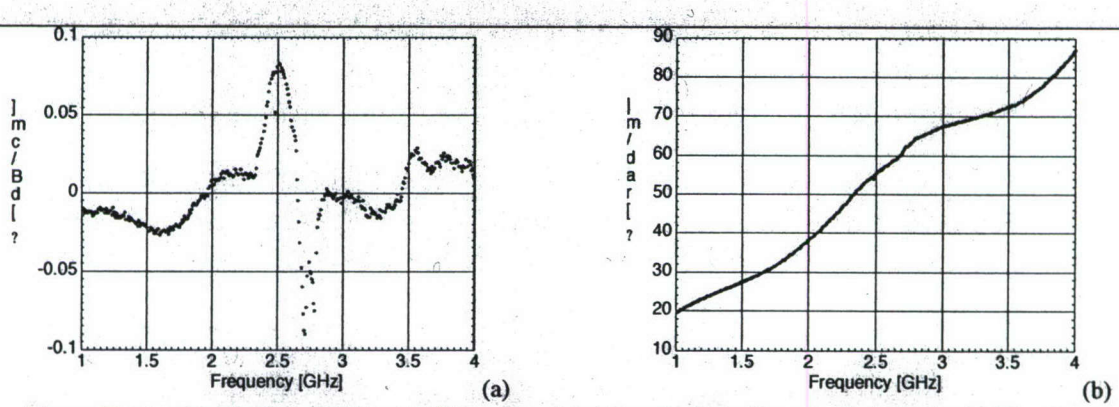

Figure 12. (a) Attenuation constant and (b) propagation constant of the line standard filled with Fluorinert.

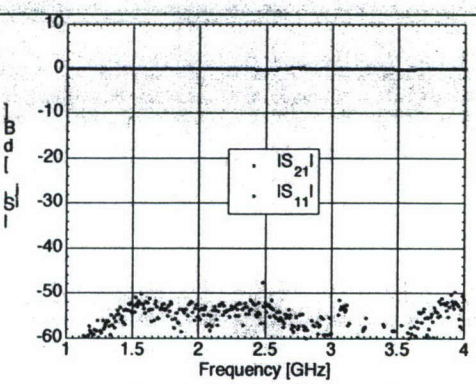

Figure 13. Magnitude of S_{21} and S_{11} of the line standard when filled with 1 mg/mL NMPs inside Fluorinert.

Sponsoring Agency: DOD AFOSR
Award Number: FA9550-07-1-0002

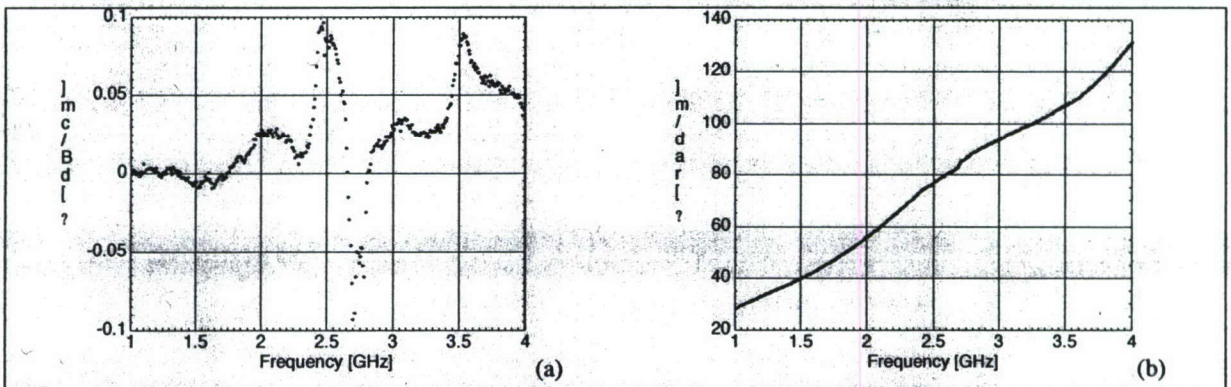

Figure 14. (a) Attenuation and (b) propagation constants of the line standard when filled with 1 mg/mL NMPs in Fluorinert.

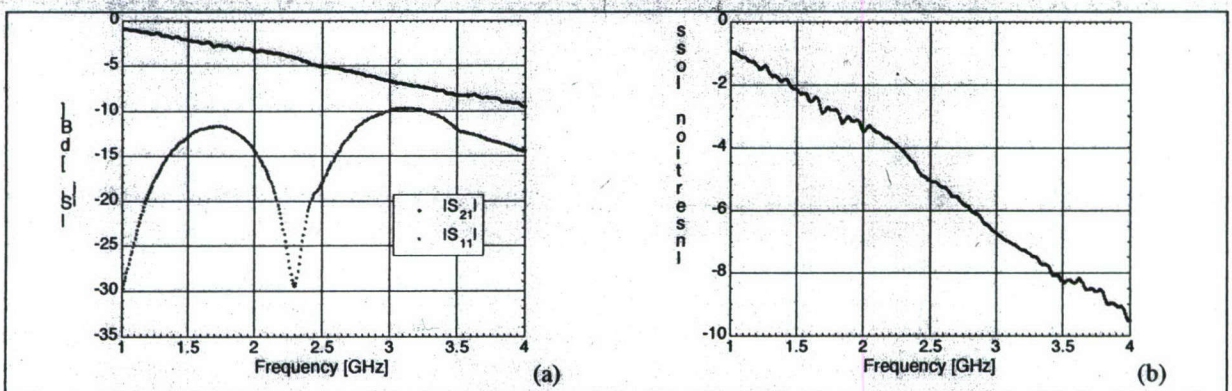

Figure 15. (a) S-parameters and (b) insertion loss of the line standard when the standard is filled with Fe_3O_4 1 mg/mL particles. In this case the standard is only calibrated up to the connectors with open, short ,and load calibration standards.

In order to validate the experiment another measurement was performed using pure magnetic particles (Fe_3O_4) instead of Fluorinert. This measurement was carried on the line standard and the standard was only calibrated out up to the connectors, so the length of the "line" in this experiment is equal to the physical length of the line standard (87 mm). Fig. 15(a) shows the S-parameter of this line, and Fig. 15(b) shows the insertion loss. The insertion loss is 10 dB at 4 GHz, which indicates that the addition of iron oxide to Fluorinert creates a lossy dielectric.

Microwave Measurements - Conclusions

Colloids, both magnetic (containing Fe_3O_4 or Ni) and non-magnetic (containing Cu), were characterized to determine absorptive properties. Solutions of the particles, with Fluorinert used as the suspension liquid, were measured over a wide range of frequency bands (waveguide bands D, W, K, L & S), but no significant transmission loss was noted, or any strong reflective properties. Several methods were utilized for these measurements, including various free-space Gaussian-beam systems, and a transmission-line method. In no cases were there any statistically significant differences between the solutions with nano-particles and those of unmodified Fluorinert solution. Based upon these observations, Fluorinert does possess non-lossy microwave absorption characteristics and therefore provides an ideal matrix for nanoparticulate inclusions if the matrix effects are to be suppressed in the desired technological application.

Sponsoring Agency: DOD AFOSR
Award Number: FA9550-07-1-0002

B-2. Autonomous modulation of bulk colloid properties via interface chemistry

pH Mediated Aggregation

In this section, we describe our development of a colloid titration procedure that allows control of aggregate size via changes in solution pH during processing. To characterize the aggregated nanoparticles in the colloid, we perform DLS and spin-spin proton relaxation measurements to link changes in aggregate size with magnetic behavior. Changes in magnetic nanoparticle aggregate size within the matrix should modify the measured RF absorption from the composite system. Previous work has demonstrated that the volume fraction of magnetic nanoparticles dispersed in a matrix can increase the RF absorption signal due to dipole-dipole interactions between individual particles in an aggregate and spin coupling between particle aggregates [10]. As a consequence, SPM nanoparticles such as Fe3O4 in the aggregated state possess higher magnetization that induces a faster dephasing of proton spins (higher R2 relaxation rates, shorter T2 relaxation times) in the vicinity of the agglomerate [11, 12].

In the Fe_3O_4/toluene colloid, particle aggregation is achieved by lowering the pH of the toluene solution. The carboxylic acid capping agent coordinates to the surface of the metal oxide via the deprotonated carboxyl group. The bare metal oxide surface is an electron donor (Lewis base) [13], and consequently coordinates with the de-protonated heptanoic acid molecule in toluene solution. Heptanoic acid is removed from the particle surface by lowering the solution pH with a weak Lewis acid (such as acetic acid), which re-protonates the carboxyl group in toluene. As a consequence, the inherently hydrophilic surfaces of the metal oxide nanoparticles are exposed to the hydrophobic toluene solution and begin to cluster without the capping molecule, thus forming the larger nanoparticle aggregate. Conversely, the nanoparticles can be de-aggregated by titrating the Fe_3O_4/toluene colloid with a weak Lewis base (such as THF). The pH-mediated aggregation of Fe_3O_4 nanoparticles in organic solution was adapted from previously published studies on iron particle dispersion [14].

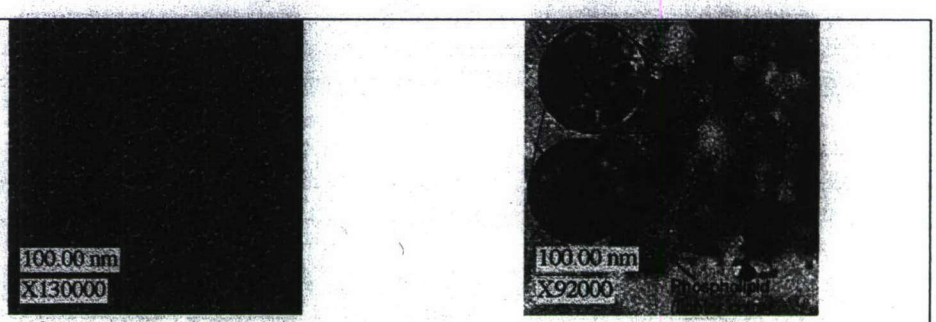

Figure 16. TEM images showing (a, left) as-synthesized 12 nanometer diameter Fe_3O_4 particles and (b, right) Fe_3O_4 nanoparticles following encapsulation in a phospholipid micelle.

The as-synthesized nanoparticles (Figure 16a) were processed in toluene at neutral and reduced pH followed by phospholipid encapsulation, yielding single and multi-particle micelles, respectively. Phospholipid micellation lends stability and water solubility for evaluation by DLS and NMR, as well as terminal functional groups for subsequent bioconjugation. In Figure 16b, single particles processed at neutral pH are shown following micelle encapsulation. The DLS size distribution results shown in Table 1 demonstrate pH dependent aggregation of Fe_3O_4 nanoparticles encapsulated in phospholipid micelles. The ~16 nm mean sample diameter is consistent with monodisperse single particle micelles with a magnetite core of approximately 12-14 nm (Figure 16b). A ~ 52 nm mean sample diameter is consistent with nanoparticle aggregates containing approximately 48 nanoparticles each, assuming a packing fraction of 0.74 (close-packed) and individual particle diameters between 12-14 nm.

T2 relaxation results for the single and multi-particle micelles shown in Figure 17 demonstrates the enhanced molar T2 relaxation rate of the multi-particle micelles compared to single particle micelles. The 368 $sec^{-1} \cdot mol^{-1}$ T2 relaxation rate of the multi-particle micelle sample shows a 22% increase compared to the 303 $sec^{-1} \cdot mol^{-1}$ T2 relaxation rate for the single particle micelle sample. The molar relaxation rates were obtained from the linear fits of the inverse T2 measurements for three Fe_3O_4 micelle dilutions. Both linear fits demonstrated near ideal correlation

(R2 > 0.9). As demonstrated by the plot in Figure 17, the larger aggregate of magnetic material per micelle in water yields a higher molar relaxation rate than the single nanoparticle per micelle colloidal sample.

% of Acetic Acid in THF (vol/vol)	*Aggregate Hydrodynamic Diameter* (normalized to one particle)
0.00%	1.0 +/- 0.010
0.23% +/- 0.04%	2.0 +/- 0.025
0.33% +/- 0.03%	5.3 +/- 0.006
0.41% +/- 0.03%	5.8 +/- 0.009
0.47% +/- 0.03%	6.4 +/- 0.005
0.52% +/- 0.02%	5.8 +/- 0.015

Table 1. Tabulated hydrodynamic diameters and variances obtained by DLS of magnetic nanoparticle aggregation in THF during titration with acetic acid. Aggregate diameters are normalized to the diameter of a single nanoparticle.

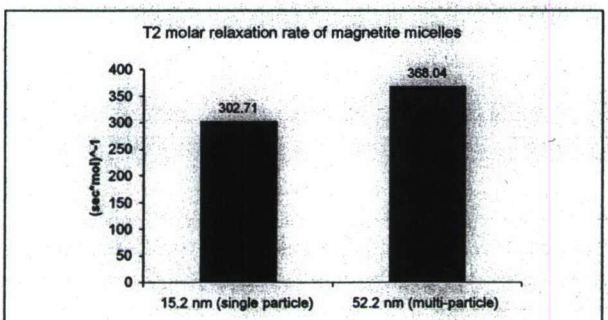

Figure 17. Hydrodynamic diameter (nm) of the Fe_3O_4 nanoparticle micelles plotted versus T2 molar relaxation rate. The larger nanoparticle aggregate yields a higher molar relaxation rate than individual particles.

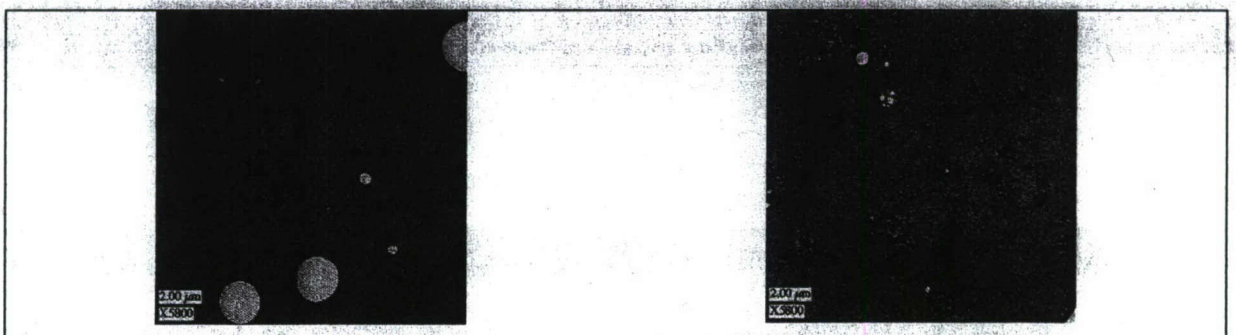

Figure 18. TEM images showing DNA mediated aggregation of micelle-encapsulated particles (a, left) before hybridization and (b, right) after hybridization. In (b), fractal aggregates larger than 1μm in diameter are observed.

Sponsoring Agency: DOD AFOSR
Award Number: FA9550-07-1-0002

DNA-mediated nanoparticle aggregation

In this section, we describe a second experimental approach for promoting nanoparticle aggregation in the colloidal solution mediated by DNA. Several studies have investigated the bimolecular driven aggregation of micro and nanoparticles in solution [11, 15]. In our case, particle aggregation is desired to modulate local number concentration and in turn RF absorption in the colloidal solution. Of particular interest is exploring the use of single-stranded DNA (ssDNA) to drive particle aggregation. Because there is a very well defined relationship between DNA sequence and the thermodynamics of double-stranded DNA (dsDNA) formation, it is possible to control the aggregation of particles using sequence specificity [11]. dsDNA melting transitions are well defined and correlate with the DNA nucleotide sequence. Melting temperatures increase with increasing DNA strand length and with increasing GC base content, and are easily calculated from the sequence using pair wise interaction parameters [16]. The melting transitions of these dsDNA are typically broad and occur over a temperature range of ~20°C. Recently it has been observed that dsDNA transitions in micro- or nanoparticle aggregates show sharp thermal transitions of a few degrees or less [17, 18], with time constants in the millisecond range for sufficient temperature jumps [19]. Thus, the DNA driven aggregation, thermal melting, and dissolution of colloidal nanoparticles can be controlled over a very sharp thermal range yielding reversible changes in particle volume fraction.

In the work reported here, we link ssDNA to a population of micelle-encapsulated particles via carboxyl functional groups on the phospholipid molecules. The complimentary ssDNA to the former is bound to a second population of micelle-encapsulated particles. Upon mixing of the two populations in the colloidal solution at 20°C, the complimentary DNA strands hybridize, thus promoting aggregation below the melting transition of the dsDNA. By varying the ratio of ssDNA per micelle, the ultimate size of the aggregate can be tailored. For example, by maximizing the number of ssDNA attached to each population (saturation of ssDNA per micelle), aggregation is not well-controlled and extremely large aggregate networks form. Figure 18 shows TEM images before and after DNA hybridization and formation of fractal aggregates with sizes in excess of 1 μm.

In order to demonstrate precise control of the bioconjugation process and aggregate formation, ssDNA was linked to micelle-encapsulated particles as described in Section 3.1 in ratios of one strand per micelle (1:1) and 2.5 strands per micelle (2.5:2.5) on average. Figure 6 shows size data obtained by DLS for samples with no aggregation, and micelle-encapsulated particle populations with 1:1 and 2.5:2.5 DNA additions per micellated particle. For the case of moderate aggregation, a 1:1 DNA to micelle ratio should yield on average only two micelles per aggregate, while a 2.5:2.5 DNA to micelle ratio should yield a larger aggregate. The results shown in Figure 19 support this conclusion, as the (1:1) sample has a hydrodynamic diameter 50% greater than the unhybridized micelle, indicative of the decreased diffusion coefficient of aggregated particles. Similarly, the (2.5:2.5) sample has a hydrodynamic diameter nearly 150% greater than the unhybridized micelle, demonstrating increased aggregation. These results indicate that DNA can be utilized as a selective surface ligand on nanoparticles to precisely control the degree of aggregation in colloidal systems.

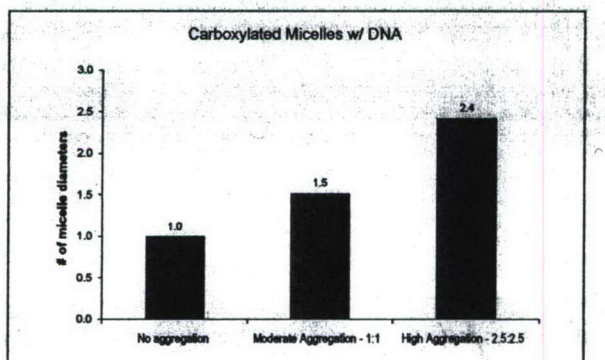

Figure 19. DLS results for particle micelles conjugated with varying quantities of complimentary DNA. Note that the diameters are normalized to diameter of single micelles.

Sponsoring Agency: DOD AFOSR
Award Number: FA9550-07-1-0002

Autonomous Colloidal Aggregation – Conclusions

In this work, two routes to the controlled aggregation of nanoparticulate inclusions in a colloidal solution have been demonstrated. In both scenarios, nanoparticle interface chemistry is used to dictate the degree of aggregation without the application of external mechanical or electrostatic actuation. In the first case, we utilized a pH change in the colloidal solution and acid-base interaction of the molecular capping layer to drive nanoparticle aggregation (and dispersion). T2 relaxation measurements on the resulting aggregates demonstrate magnetic property changes with local nanoparticle concentration. In the second case, we demonstrated aggregation in the colloid via the hybridization of complimentary ssDNA covalently bound to the surfaces of two particle populations. The ultimate aggregate size and shape is controlled by the amount of ssDNA per particle, thus demonstrating that aggregate size can be precisely tailored via the addition of a site-specific biological ligand such as DNA. In principle, both of the interface chemistries demonstrated in this paper are both passive and reversible. While we were unable to demonstrate these approaches in the modulation of microwave absorption/reflection in colloidal solutions, this work does demonstrate the feasibility of modulating bulk colloid properties via microscopic changes at the nanoparticle surface, i.e., molecular exchange or DNA hybridization. In addition, this approach will work for the modulation of EM waves with shorter wavelengths, such as UV-visible and IR, and may therefore have potential applications for technologies beyond radio frequencies.

B-3. Microfluidic Modeling for Active Modulation of Microwave Absorption using Colloidal Solutons

The Berkeley group has focused their efforts on an approach to self-pump fluids through microchannels making use of surface tension forces developed across a liquid-vapor interface. Figure 20 shows a rough schematic of how such a device would work.

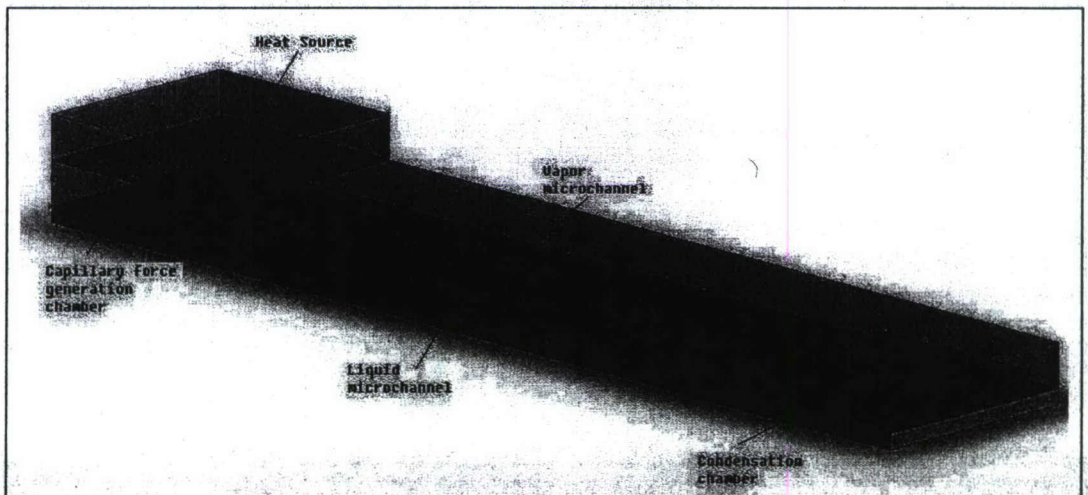

Figure 20. Pumping liquid through a microchannel using unequal capillary forces at its two liquid-vapor interfaces

The setup consists of a Capillary force generation (CFG) chamber at one end of one or more liquid microchannels and a condensation chamber on the other end. A vapor microchannel provides a separate connection between the CFG and condensation chambers. The fluid in the CFG chamber is evaporated using a heat source to create a liquid-vapor interface. The capillary pressure drop across such an interface is given by

$$\Delta P = \frac{2\gamma}{R}$$

where γ is the surface tension and R is the radius of curvature of the interface. The CFG chamber is packed with a wick structure whose small radii pores give rise to large pressure drops across this interface. The evaporated vapor continues in the vapor microchannel until it condenses in the condensation chamber leading to another vapor-liquid interface with a large radius of curvature and thus minimal capillary pressure drop. This difference in pressure drops at the two interfaces gives rise to fluid motion in the liquid microchannels. The capillary forces are in turn countered

by the liquid and vapor flow pressure drops in the channels and wick, leading to a steady state fluid flow. A numerical model was created to estimate the flow rate of the liquid in the microchannels as a function of different parameters including device dimensions and fluid properties. Figure 21 shows how mass flow rate depends on the wick pore size with other design parameters held constant. This model can be used to optimize design parameters or to test device performance. The mass flow rate basically increases with heat input from the heat source though the exact relationship would be determined by a numerical model. In this way we would be able to self pump fluid in the microchannels by providing a temperature gradient between the CFG and condenser chambers.

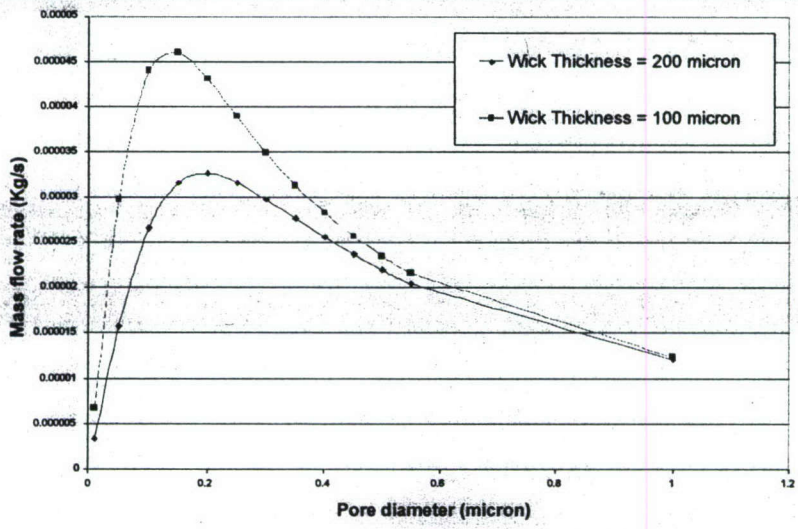

Figure 21. Variation of the mass flow rate with wick pore size for two different wick thicknesses with all the other design parameters held constant

Microfluidic for Active Modulation – Conclusions

Initial modeling results indicate that the previously described 'self-pump' process is viable for an autonomous fluid delivery system (i.e., for the wing of an UAV). Other work has explored the development of a Teflon based injection molding process and preliminary evaluation of material and process requirements are favorable. Finally, Fluorinert droplet formation has been demonstrated using a prototype microfluidic device.

C. Project Summary and Conclusions

The overall objective of this DARPA seed grant project was not achieved as proposed. That is, the project team was not able to demonstrate microwave absorption and modulation using colloidal solutions containing nano-magnetic materials. While support for this approach in the literature database is limited, available studies for comparison [6, 9] indicate that very high particle loads (as high as 30% v/v) may be required to achieve microwave absorption/reflectivity. Our work demonstrates that particle volume fractions up to 10% do not have a microwave absorption cross-section. Stable particle volume fractions above 10% could not be achieved in our laboratory through the modification of particle size, ligand type/length, and solution type. In every case, particle segregation and precipitation was observed above 10% v/v. More work is necessitated to identify the necessary colloid characteristics that will permit the formulation of highly concentrated colloids with particle fractions above 10% v/v. While microwave wavelengths are determined to be insensitive to dilute colloidal solution, we note that shorter wavelengths (e.g., UV-visible, IR, etc.) will be sensitive to nanometer scale particles. As a consequence, we believe that similar approaches to modulation of bulk properties can be pursued for other technologies operative at different wavelengths. One obvious example is invisibility, which depends on the modulation of visible wavelengths of light.

Sponsoring Agency: DOD AFOSR
Award Number: FA9550-07-1-0002

D. References Cited

[1] M. D. Bushbeck and C. H. Chan, "A tuneable, switchable dielectric grating," Microwave and Guided Wave Letters, IEEE [see also IEEE Microwave and Wireless Components Letters], vol. 3, pp. 296-298, 1993.

[2] M. Bushbeck, "Electromagnetic scattering from a two-state phase switched screen using a control impedance," 2004.

[3] P. V. Wright, B. Chambers, A. Barnes, K. Lees, and A. Despotakis, "Progress in smart microwave materials and structures," Smart Materials & Structures, vol. 9, pp. 273-279, 2000.

[4] R. Zhang, A. Barnes, K. L. Ford, B. Chambers, and P. V. Wright, "A new microwave 'smart window' based on a poly(3,4-ethylenedioxythiophene) composite," Journal of Materials Chemistry, vol. 13, pp. 16-20, 2003.

[5] M. Wilson, "Designer materials render objects nearly invisible to microwaves," in Physics Today, vol. 60, 2007, pp. 19-23.

[6] V. B. Bregar, "Advantages of ferromagnetic nanoparticle composites in microwave absorbers," Magnetics, IEEE Transactions on, vol. 40, pp. 1679-1684, 2004.

[7] V. B. Bregar, "Effective-medium approach to the magnetic susceptibility of composites with ferromagnetic inclusions," Physical Review B (Condensed Matter and Materials Physics), vol. 71, pp. 174418-8, 2005.

[8] R. P. Pant, S. K. Halder, S. K. Dhawan, J. Shah, V. Kumar, and N. D. Kataria, "Microwave Absorption Studies on Ferrofluid-Conducting Polymer Composite," presented at XXVIIIth General Assy of Int'l Union of Radio Science, New Dehli, India, 2005.

[9] M. S. Pinho, M. L. Gregori, R. C. R. Nunes, and B. G. Soares, "Performance of radar absorbing materials by waveguide measurements for X- and Ku-band frequencies," European Polymer Journal, vol. 38, pp. 2321-2327, 2002.

[10] N. Guskos, J. Typek, T. Bodziony, Z. Roslaniec, U. Narkiewicz, M. Kwiatkowska, and M. Maryniak, "Temperature dependence of FMR field of magnetic nanoparticles/polymer composite," Reviews on Advanced Materials Science, vol. 12, pp. 133-138, 2006.

[11] J. M. Perez, L. Josephson, T. O'Loughlin, D. Hogemann, and R. Weissleder, "Magnetic relaxation switches capable of sensing molecular interactions," Nature Biotechnology, vol. 20, pp. 816-820, 2002.

[12] A. Roch, R. N. Muller, and P. Gillis, "Theory of proton relaxation induced by superparamagnetic particles," Journal of Chemical Physics, vol. 110, pp. 5403-5411, 1999.

[13] E. Johansson and L. Nyborg, "XPS study of surface-active organic compounds on fine ferrous powder," Surface and Interface Analysis, vol. 30, pp. 333-336, 2000.

[14] W. J. Chen, S. S. Wong, W. G. Peng, and C. D. Wu, "Effect of Acid-Base Interaction on Magnetic Dispersion Containing Alpha-Fe Metal Particles," Ieee Transactions on Magnetics, vol. 27, pp. 4648-4650, 1991.

[15] T. A. Taton, C. A. Mirkin, and R. L. Letsinger, "Scanometric DNA array detection with nanoparticle probes," Science, vol. 289, pp. 1757-1760, 2000.

[16] H. T. Allawi and J. SantaLucia, "Thermodynamics and NMR of internal GT mismatches in DNA," Biochemistry, vol. 36, pp. 10581-10594, 1997.

[17] H. Long, M. Chen, and G. C. Schatz, "Cooperative DNA Melting in DNA Linked Gold Nanoparticle Aggregates," presented at Foundations of Nanoscience, Self-Assembled Architectures and Devices, Snowbird, UT, 2004.

[18] F. Pierce, C. M. Sorensen, and A. Chakrabarti, "Aggregation-Fragmentation in a Model of DNA-Mediated Colloidal Assembly," Langmuir, vol. 21, pp. 8992-8999, 2005.

[19] U. Christensen, N. Jacobsen, V. K. Rajwanshi, J. Wengel, and T. Koch, "Stopped-flow kinetics of locked nucleic acid (LNA)-oligonucleotide duplex formation: studies of LNA-DNA and DNA-DNA interactions," Biochem J, vol. 354, pp. 481-4, 2001.